MRS-Tex: A Magnetically Responsive Soft Tactile Device for Texture Display

Yuan Guo, Qianqian Tong, Xianzhong Liu, Xuesong Bian, Zhihao Zhang, Yuru Zhang, *Senior Member, IEEE*, Weiliang Xu, *Senior Member, IEEE*, Dangxiao Wang*, *Senior Member, IEEE*

***Abstract*—Tactile devices provide an intuitive way for texture display, which allows users to perceive the detailed surface properties of virtual or remote objects. For existing tactile devices that create actual topographical transformations, it remains challenging to render surface textures with high spatial resolution due to the limitation of the size of actuators. To address this challenge, a magnetically responsive soft actuator with a diameter of 1 mm is proposed. Integrating the high-density soft actuator array and a soft membrane bracket, we develop a magnetically responsive soft tactile device (named MRS-Tex) for texture display. When a magnetic field is applied, the magnetic units will sink to form pits, and the soft membrane bracket resists the finger pressure so that users can perceive the rendered surface texture. Thanks to the proposed sunken solution, MRS-Tex is capable of rendering surface textures with millimeter-level resolution (1.5 mm) while providing the sufficient upward holding force. Moreover, we conduct quantitative experiments and two user studies to evaluate the performance of MRS-Tex. Experimental results show that MRS-Tex can generate pits with a depth of more than 0.20 mm, which is sufficient for rendering perceivable surface textures. The average discrimination accuracy of user study can reach up to 82% for both six basic texture patterns and four complex texture patterns.**

***Index Terms*—Magnetic soft materials, soft actuator array, surface texture, texture display, tactile device.**

I. Introduction

As one of the most important sensory functions for human perception, tactile perception not only endows us the ability to interact with the physical world, but also significantly enriches our daily life, playing an important role in a wide range of applications such as robotics, wearable devices, and health care [1-7]. In the real world, humans perceive tactile information mainly through the surface texture of objects, making it easy to discriminate huge varieties of fabrics, appreciate delicate sculptures, and read braille books [8].

The surface texture of an object is characterized by its surface morphology in terms of continuous micro-scale changes in height. The relative height difference between adjacent positions forms uneven grooves. To present the texture information to a user, different technologies have been developed to design tactile devices for texture display. According to the operating principle, the existing tactile devices can be categorized to the one simulating the perception of texture change via sensory manipulation for tactile feedback, and the other physically forming actual topographical features on the device surface for texture perception.

Many techniques have been developed for texture display via sensory manipulation, such as electrotactile effects (i.e., vibration-like sensations due to the electrostimulation between the wired electrode and the skin) [9], electrostatic adherence [10-12], piezoelectric effects [13, 14], surface acoustic waves [15, 16], etc. These techniques simulate texture changes without creating actual topographical transformations, making it difficult to produce localized tactile feedback. Furthermore, due to differences in individual skin characteristics, some users cannot effectively perceive the texture information using these techniques. For example, when using electrostatic devices, some users' perception ability is greatly affected by the cuticle thickness and wettability of their fingertip skin.

To overcome the shortcomings of the abovementioned techniques, some researchers resorted to physically form actual topographical features for texture display. The actuation methods for this purpose include electroactive actuators [17], pneumatic actuators [18], shape memory polymer actuators [19], artificial muscles [20], etc. These methods form textures by raising certain units under the actuation of actuators. As mentioned in [21], the target resolution is 1 mm for an ideal tactile device. Limited by the size of actuators, however, the tactile devices in [17-20] have a resolution greater than 3 mm. It remains a challenge to design a smaller actuator required for tactile devices with higher spatial resolution.

Stimuli-responsive materials have attractive potential in designing and fabricating miniaturized actuators, such as light

Manuscript received Month xx, 2xxx; revised Month xx, xxxx; accepted Month x, xxxx.

This work is supported by the National Key Research and Development Program under Grant No. 2017YFB1002803, by the National Natural Science Foundation of China under Grant 61973016, and by the China Postdoctoral Science Foundation under Grant No. 2019M663018.

Yuan Guo, Xianzhong Liu, Xuesong Bian, Zhihao Zhang, Yuru Zhang, and Dangxiao Wang are with the State Key Lab of Virtual Reality Technology and Systems and Beijing Advanced Innovation Center for Biomedical Engineering, Beihang University, No. 37 Xueyuan Road, Haidian District, Beijing 100191, China.

Qianqian Tong and Dangxiao Wang are with Peng Cheng Laboratory, Shenzhen 518055, China.

Weiliang Xu is with the Department of Mechanical Engineering, University of Auckland, New Zealand.

Corresponding author: Dangxiao Wang, Email: hapticwang@buaa.edu.cn.

This article has been accepted for publication in a future issue of this journal, but has not been fully edited. Content may change prior to final publication. Citation information: DOI 10.1109/TIE.2021.3120490, IEEE Transactions on Industrial Electronics

[22, 23], temperature [24], and magnetic materials (magnets, coils, or magnetic soft materials) [25-27]. Among them, magnetic soft materials have been widely used in soft robots, drug delivery, medical applications, etc. [27-29]. Under applied magnetic fields, the magnetic particles embedded in the magnetic soft materials can be regarded as distributed actuation sources, which enables the actuator readily to reach millimeter level. Inspired by this advantage, we design a flexible magnetic unit (named magnetically responsive soft actuator, MRSA) for the tactile device. Nevertheless, the MRSA is soft, failing to provide a sufficient upward holding force (100 mN) [19, 30] to resist users' finger pressure like the existing actuators [17-19].

Observing that textures of an object surface can be profiled by both concave and convex, we propose a sunken solution in which concave rather convex is formulated to generate geometric profiles encoded in the target texture pattern. In other words, due to the concave forming pit on the surface, the MRSA does not need to provide the upward holding force to resist the pressure exerted by fingers. Combining a number of MRSAs with a thin film, we prepare a MRSA array arranged in a certain manner. Integrating the MRSA array with the specifically designed soft membrane bracket, a novel magnetically responsive soft tactile device (named MRS-Tex) is proposed for texture display. Under the applied magnetic field, magnetic units arranged in a pre-defined manner can form a specific pattern of pits, producing the desired texture on the surface of MRS-Tex. Benefiting from the advantage that MRSA can be easily miniaturized, MRS-Tex has a millimeter-level spatial resolution (1.5 mm).

II. Working Principle and Fabrication Processes

A. Working principle of MRS-Tex

MRS-Tex for texture display is composed of ferromagnetic materials and soft polymer. Specifically, the magnetized or magnetizable particles (namely ferromagnetic materials) are uniformly embedded in the soft polymer. Exploiting magnetic forces generated from the embedded particles under applied magnetic fields, magnetic soft materials can be remotely actuated and controlled accurately.

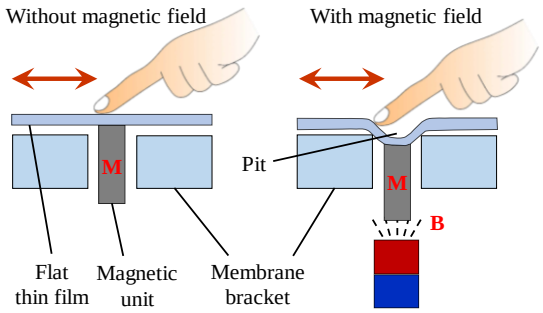

Fig. 1. Working principle of our MRS-Tex producing deformation in vertical direction.

The principle of MRS-Tex is depicted in Fig. 1, where the magnetic units adhered with the thin film are assembled into the membrane bracket. At the initial state, the magnetic units are not in action, and the thin film is completely flat. While excited by an applied magnetic field, the magnetic units sink a certain distance, thus creating a pit on the thin film. In this way, a pattern of pits can be formed to represent a desired texture pattern on the MRS-Tex. When the magnetic field is removed, the magnetic units return to the initial state due to the elastic thin film. Compared with the existing tactile devices [17-19], MRS-Tex provides an upward holding force via the membrane bracket rather than via the actuators. Therefore, the actuators of MRS-Tex can be designed to be relatively small to meet the requirement of high spatial resolution.

B. Fabrication of MRSA array

The fabrication process for the MRSA array is depicted in Fig 2. First, Part A and Part B of Ecoflex 00-30 (Smooth-On Inc., USA) are mixed in a 1:1 mass ratio (Fig. 2(a)). Magnetic neodymium-iron-boron (NdFeB) particles with an average size of 5 μm (LW-BA-16-7A-2000, Guangzhou Xinnuode Transmission Parts Co., Ltd, China) are then added into the mixed Ecoflex to obtain the composite ink (Fig. 2(b)). Next, the

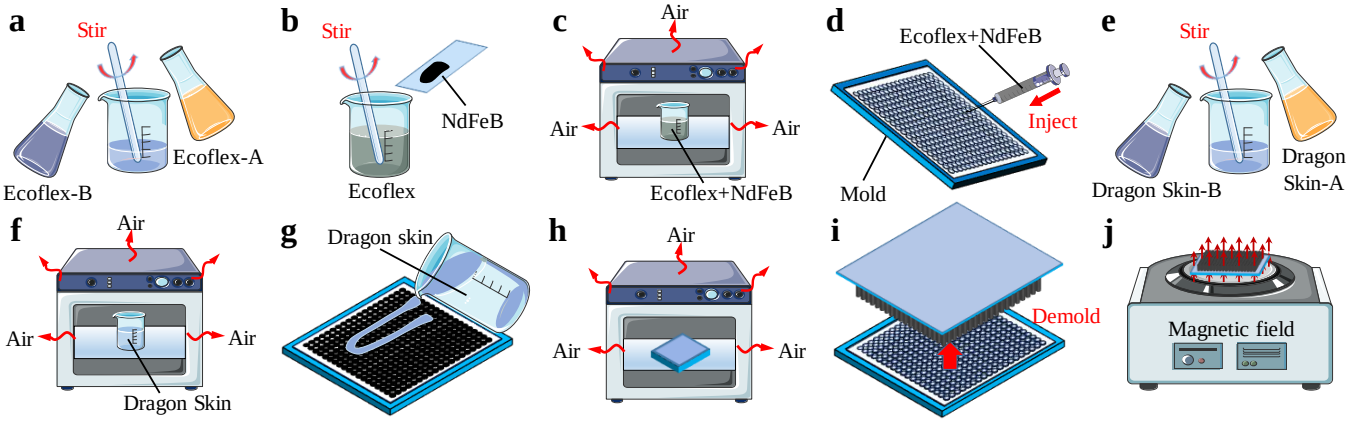

Fig. 2. Fabrication process of MRSA array. (a) Mixing two components of Ecoflex. (b) Adding NdFeB particles into the mixed Ecoflex to prepare composite ink. (c) Evacuating air from composite ink. (d) Injecting composite ink into the holes of a 3D printed mold and then curing for five hours. (e) Mixing two components of Dragon Skin. (f) Evacuating air from mixed Dragon Skin. (g) Pouring mixed Dragon Skin onto the top surface of the 3D printed mold to form a thin film. (h) Evacuating air from thin film and curing for five hours. (i) Demolding process of cured MRSA array. (j) Magnetization process of MRSA array.

This article has been accepted for publication in a future issue of this journal, but has not been fully edited. Content may change prior to final publication. Citation information: DOI 10.1109/TIE.2021.3120490, IEEE Transactions on Industrial Electronics

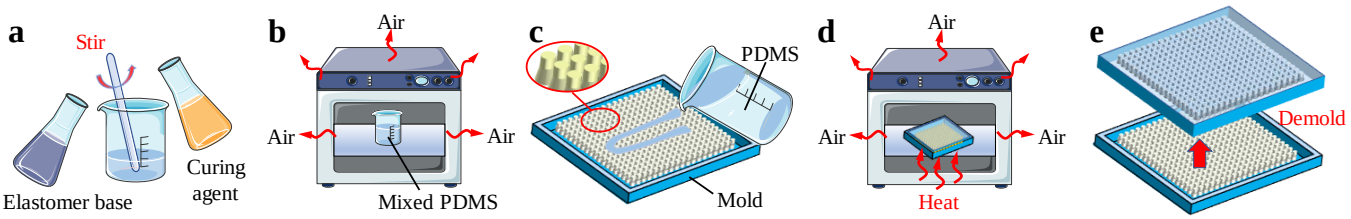

Fig. 3. Fabrication process of soft membrane bracket. (a) Mixing elastomer base and curing agent of PDMS. (b) Evacuating air from mixed PDMS. (c) Pouring PDMS into a 3D printed mold. (d) Evacuating air again and heating for five hours in a vacuum furnace. (e) Demolding the soft membrane bracket from the 3D printed mold.

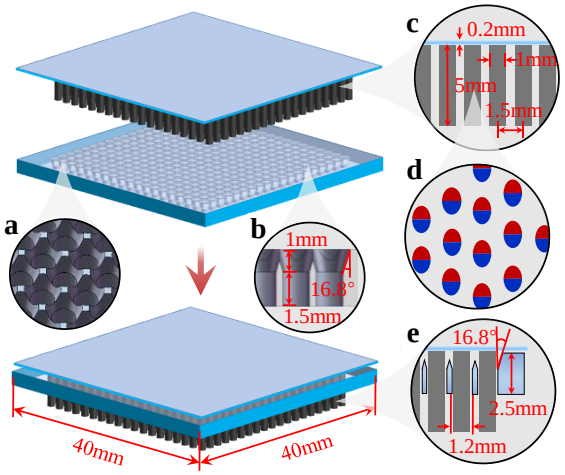

Fig. 4. Overall structure of the proposed MRS-Tex. The inset figures show the magnified image of (a) the local structure of soft membrane bracket, (b) the cross section of soft membrane bracket, (c) the cross section of MRSA array, (d) the arrangement of magnetic particle (red is N polar and blue is S polar), and (e) the cross section of MRS-Tex.

well-mixed composite ink is evacuated in a vacuum furnace until the air bubbles are no longer visible (Fig. 2(c)). After that, the composite ink is injected into a 3D printed mold to form unmagnetized units (Fig. 2 (d)).

Once the composite ink is cured, the Dragon Skin 10 (Smooth-On Inc., USA) mixed by Part A and Part B with a 1:1 mass ratio is evacuated for 10 min to remove the air bubbles (Fig. 2 (e) and Fig. 2(f)). Then the mixed Dragon Skin 10 is poured onto the top surface of the 3D printed mold to prepare the thin film (Fig. 2 (g)). The thin film with a thickness of approximately 0.2 mm adheres automatically to the magnetic units to form a whole MRSA array. After vacuuming, the MRSA array is cured for five hours (Fig. 2(h)). Subsequently, the cured MRSA array is peeled off from the 3D printed mold and magnetized using a magnetizer (Shenzhen Jiuju Industrial Equipment Co., Ltd, China), thereby imparting magnetic polarities to the ferromagnetic particles embedded in the Ecoflex 00-30, as shown in Fig. 2(i) and (j).

C. Fabrication of soft membrane bracket

The fabrication process of the soft membrane bracket is similar to that of the MRSA array. As illustrated in Fig. 3(a), the two components of polydimethylsiloxane (PDMS) (Sylgard 184, Dow Corning Corp., USA) are mixed in a mass ratio of 1:10. Then, the well-mixed PDMS is placed in a vacuum furnace to remove air bubbles (Fig. 3(b)). Subsequently, the soft membrane bracket is created by pouring the well-mixed PDMS into a 3D printed mold (Fig. 3(c)). The 3D printed mold containing the well-mixed PDMS is vacuumed again to ensure that the poured model is free of air bubbles, and then is cured in a vacuum furnace for 5 hours at 60°C (Fig. 3(d)). Finally, the cured soft membrane bracket is peeled off from the 3D printed mold (Fig. 3(e)), and its thickness is around 2.5 mm (Fig. 4(e)).

To increase the pit depth, we optimize the design of the soft membrane bracket. The upper part of the hole on the soft membrane bracket (Fig. 3(c)) is designed to be the frustum of a cone (Fig. 4(a) and (b)) instead of a cylinder, and the angle between the generatrix and the vertical plane is 16.8°. Therefore, when the magnetic unit moves downward, a large area of thin film connected around the magnetic unit will sink to form a larger concave deformation, so that the pits are more easily perceived by users.

D. Overall design of MRS-Tex

After the above fabrication process, the MRSA array and soft membrane bracket are assembled into MRS-Tex. As shown in Fig. 4, the device integrates a 19 × 19 MRSA array with a total size of 40 mm × 40 mm. The magnetic units are spaced 1.5 mm apart, and each magnetic unit is 1 mm in diameter and 5 mm in height (Fig. 4(c)). The diameter difference between the magnetic unit and the hole of the membrane bracket is 0.2 mm (Fig. 4(c) and (e)). The height of the frustum of the cone (upper part of the hole) and the cylinder (lower part of the hole) are 1 mm and 1.5 mm, respectively (Fig. 4(b)).

When the geometric parameters of MRS-Tex are determined, the pit depth depends on the magnetic force. Further, the magnetic force is jointly determined by the magnetization of the magnetic unit and the magnitude of the applied magnetic field. The magnetization of the magnetic unit is affected by the mass fraction of magnetized NdFeB particles in the composite ink. With the increase of the mass fraction, the magnetization of the magnetic unit also increases. Similarly, the pit depth is positively correlated with the applied magnetic field. The greater the applied magnetic field strength, the deeper the pit depth. Consequently, a certain depth of the pit can be obtained by regulating the applied magnetic field. The applied magnetic field can be generated by an electromagnetic coil or an NdFeB magnet. The electromagnetic coil connected with a constant current power supply is used for the quantitative performance experiments (in Section III), and the magnetic field of the electromagnetic coil is adjusted by manually regulating the current of the power supply. The NdFeB magnet with a surface flux density of 300 mT is placed on the experimental setup and is used for user evaluation (in Section IV-B).

This article has been accepted for publication in a future issue of this journal, but has not been fully edited. Content may change prior to final publication. Citation information: DOI 10.1109/TIE.2021.3120490, IEEE Transactions on Industrial Electronics

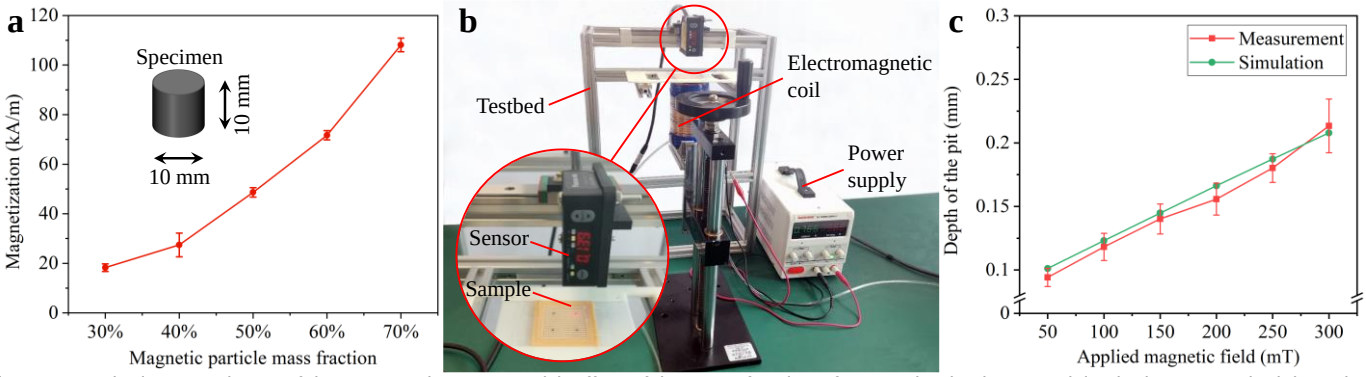

Fig. 5. Quantitative experiment of the proposed MRS-Tex. (a) Effect of the mass fraction of magnetized NdFeB particles in the composite ink on the magnetization of magnetic samples. (b) Experimental setup for measuring the depth of pits. (c) Comparison of the measurement results and simulation prediction of the depth of pits under different applied magnetic field (for the isolated magnetic unit).

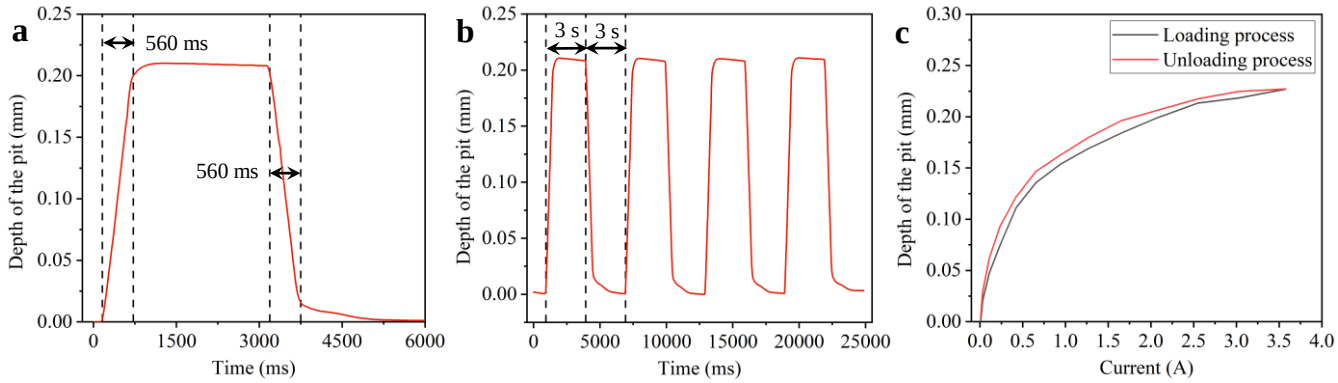

Fig. 6. The dynamic performance of the tactile device. (a) Response time. (b) Repeatability. (c) Hysteresis.

III. Validation of MRS-Tex

A. The magnetization of magnetic units

The mass fraction of magnetized NdFeB particles in the composite ink is a dominant factor in maximizing the magnetization of magnetic units. As such, we prepared five kinds of magnetic samples with the same size (10 mm in diameter and 10 mm in height) and different NdFeB particle content. The mass fraction of magnetized NdFeB particle and composite ink are 30%, 40%, 50%, 60%, and 70%, respectively. We measured the magnetization of these samples using the Hysteresisgraph (MATS-2010H, Hunan Linkjoin Technology Co., Ltd, China), and the measured values of magnetic samples with the same NdFeB particle content were averaged.

As shown in Fig. 5(a), as the mass fraction of magnetized NdFeB particles in the composite ink increases from 30% to 70%, the magnetization of magnetic samples varies almost linearly from 18.25 kA/m to 108.14 kA/m. However, when the mass fraction is higher than 60%, the rheological property of the composite ink will become poor, making it difficult to inject the composite ink into the mold. Considering both the difficulty of the fabrication process and the magnetization of magnetic units, we chose the composite ink with 60 wt% NdFeB particles to prepare the MRSA array.

B. The depth of pits

As mentioned in Section II-D, the applied magnetic field is an important factor affecting the depth of pits. To investigate the depth of pits under different applied magnetic fields, we designed an experimental setup to measure the depth of pits. As shown in Fig. 5(b), the laser displacement sensor (HL-G103-S-J, Panasonic, Japan) and the magnetized sample are fixed on the testbed. An electromagnetic coil is placed below the sample to provide the required magnetic field, which can be obtained by regulating the current of the power supply.

After the electromagnetic coil is energized, magnetic units sink a certain distance under the applied magnetic field. For the depth measurement, we selected 5 isolated magnetic units (i.e., there are no other adjacent magnetic units around each magnetic unit) with 60 wt% NdFeB particles and a height of 5 mm. The averaged depth under different applied magnetic fields is shown in Fig. 5(c). As the applied magnetic field increases from 50 mT to 300 mT, the average depth of pits increases from 0.09 mm to 0.21 mm. According to the preliminary perception experiment, the absolute threshold of the pit depth is 0.023 mm for PDMS samples with a diameter of 1 mm (in Section IV-A), demonstrating that the texture patterns rendered by MRS-Tex (0.21 mm) can be perceived by users.

In addition, we simulated the deformation of the thin film under the same condition with the above experimental setup using COMSOL (Fig. S1), and the simulation results (green line in Fig. 5(c)) are consistent with the experimental results (red line in Fig. 5(c)).

C. Dynamic performance

Using the experimental setup (Fig. 5(b)), we further evaluated the dynamic performance of MRS-Tex, including the

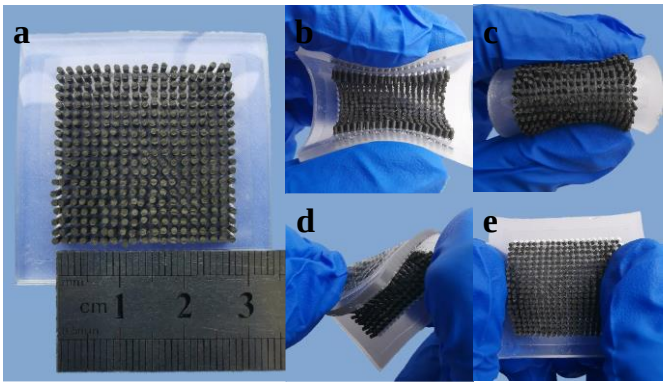

Fig. 7. Photograph of MRS-Tex showing its favorable flexibility and stretchability. (a) The prepared MRS-Tex with high spatial resolution (1.5 mm) can (b) bend inward, (c) bend outward, (d) twist, and (e) stretch.

response time, repeatability and hysteresis. In one work cycle, as the applied magnetic field increased from 0 mT to 300 mT, the pit depth formed by the isolated magnetic unit increased rapidly to 0.2 mm within 560 ms (Fig. 6(a)). After 3 s, as the applied magnetic field decreased from 300 mT to 0 mT, and the formed pit disappeared in about 560ms.

By repeating the abovementioned work cycle for several times, we can obtain the repeatability of our device (Fig. 6(b)). In different cycles, the pit depths keep almost the same both in the present and absent states of the applied magnetic field. To evaluate the hysteresis of our device, we measured the pit depths during the gradual increase (loading process) and gradual decrease (uploading process) of the current in the electromagnetic coil. As shown in Fig. 6(c), a small hysteresis was observed in the loading-uploading process, and the thin film can fully be restored to the initial state after unloading (i.e., without residual strain).

D. Flexibility and stretchability

As shown in Fig. 7(a), we prepared the MRS-Tex with a 19 × 19 MRSA array, and its overall stiffness is 2.14 N/mm (see Text S1 and Fig. S2 for details on the stiffness measurement). Compared with the absolute threshold (1.784 mm) of the pit spacing (in Section IV-A), the spacing of adjacent magnetic units is about 1.5 mm, showing that MRS-Tex can render fine textures comparable to human perception threshold.

Besides, compared with the existing tactile devices, with such small magnetic soft actuator, MRS-Tex can still robustly resist the finger pressure and support lateral motion of the fingertip along the thin film, mainly because the upward holding force is provided by the soft membrane bracket.

Benefiting from the properties of soft materials, MRS-Tex is competitive in terms of flexibility and stretchability. Fig. 7(b)-(e) depict the soft characterization of MRS-Tex. It can be seen that MRS-Tex can withstand a variety of deformation modes, such as inward bending, outward bending, twisting, and stretching. In addition, when MRS-Tex was in a curved state, the magnetic units can still sink a certain distance (0.272 mm) under the applied magnetic field of 200 mT (Fig. S3). Benefiting from such excellent soft characterization, MRS-Tex has the potential to be combined with other tactile feedback modes such as softness and shape display, so as to provide users with a rich multi-modal tactile experience in the future [8].

IV. User Evaluation

A. Absolute threshold experiment

To investigate the perception threshold of the pit depth and the pit spacing, we conducted the psychophysical experiments using the method of constant stimuli [31]. The participants were recruited from Beihang University, and signed on a written consent form after they had been informed of the objective and procedure of the experiment. None of them have any deficiency in the perception ability, and are all right-handed. The experimental procedure was approved by the State Key Laboratory of Virtual Reality Technology and Systems of China and was in accordance with ethical standards.

In the absolute threshold experiment of the pit depth, we prepared five cylindrical pits with a diameter of 1 mm and different pit depths (0.01 mm, 0.02 mm, 0.03 mm, 0.04 mm, 0.05 mm). The range of pit depths was determined by a preliminary experiment, spanning from imperceptible to almost always detected. For the absolute threshold experiment of the pit spacing, five pairs of pits were presented to the participants, each pair had two pits with the diameter of 1 mm and the concave depth of 0.2 mm. For the five pairs of pits, the spacing distance of two pits was set to 1.5 mm, 1.7 mm, 1.9 mm, 2.1 mm and 2.3 mm respectively (Fig. S4), which were selected through a preliminary experiment.

In each formal experiment, the samples (pits with different pit depths or different pit spacing) were randomly presented to each participant, and the participant perceived each sample 20 trials, a total of 100 trials [31]. On each trial, the participant slid his/her index finger back and forth in a natural and comfortable manner. After 10 trials, the participant was asked to take a two-minute break, and the entire experiment took about 50 minutes for each participant. Throughout the experiments, the participant was blindfolded to prevent the interference from the visual cues.

Six right-handed participants (aged between 24 and 32, with an average age of 27.7) took part in the absolute threshold experiment of the pit depth. For each trial, the participant verbally reported whether he/she perceived the pit, and the “yes” response means that the participant perceived a pit. According to the “yes” responses from all participants, we obtained the perceptual accuracy of pits with different pit depths (Fig. 8(a)). The logistic function was adopted to fit the data, and the pit depth corresponding to 50% perceptual accuracy was defined as the absolute threshold of the pit depth [31]. The absolute threshold of the pit depth was calculated as 0.023 mm, demonstrating that the texture patterns rendered by our device (0.21 mm) can be perceived by users.

For the absolute threshold of the pit spacing, six right-handed participants (aged between 24 and 30, with an average age of 26.3) took part in the experiment and verbally reported the numbers (one or two) of pits they perceived. Based on the data reported by participants, the perceptual accuracy corresponding to the different spacing distances of two pits is shown in Fig. 8(b). We adopted the logistic function to fit these data, and defined the spacing distance at which the perceptual accuracy is 50% as the absolute threshold [31]. As shown in Fig. 8(b), the

This article has been accepted for publication in a future issue of this journal, but has not been fully edited. Content may change prior to final publication. Citation information: DOI 10.1109/TIE.2021.3120490, IEEE Transactions on Industrial Electronics

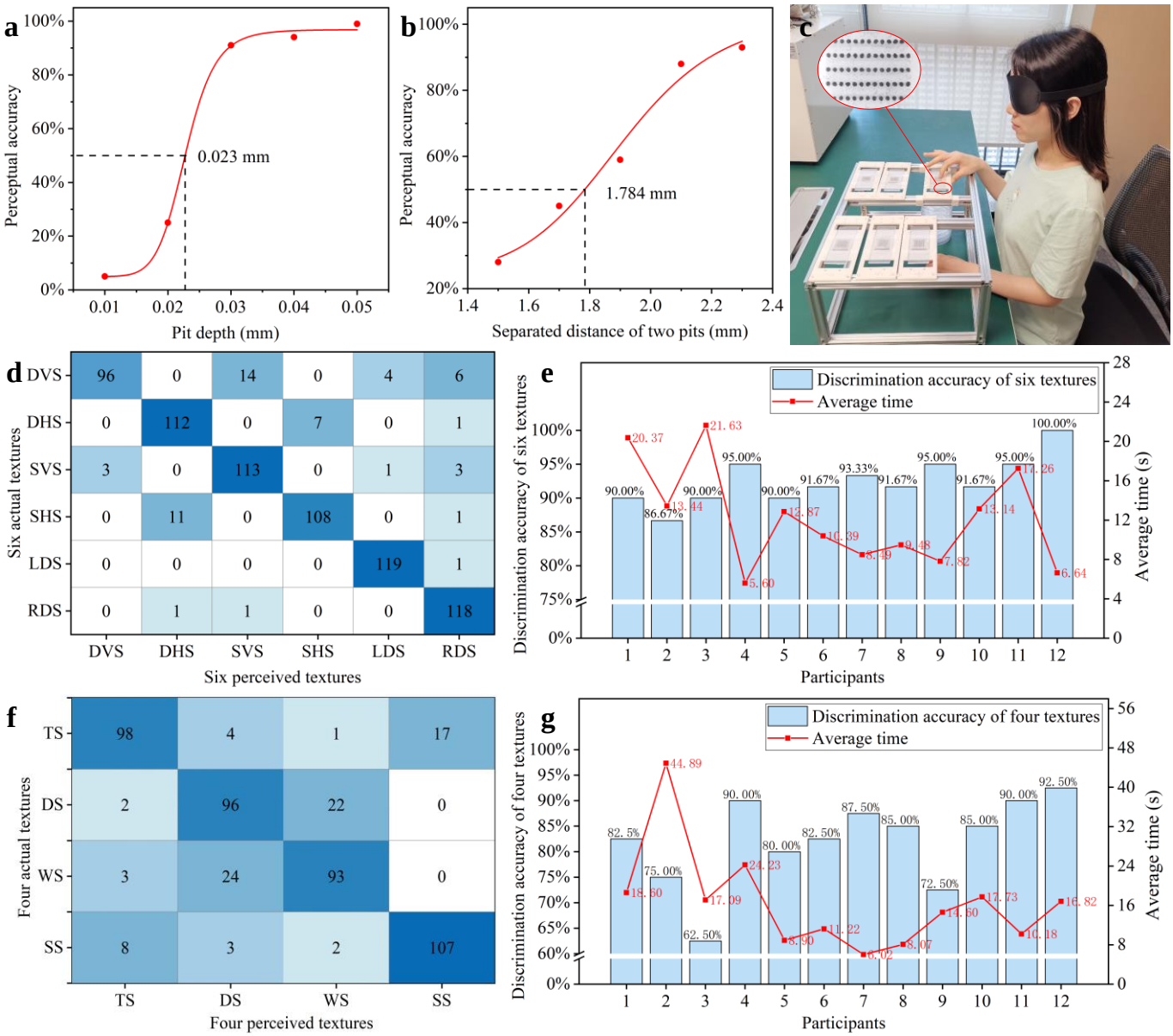

Fig. 8. User evaluation of the proposed MRS-Tex. (a) Psychometric curve with fitted function for absolute threshold experiment of pit depth. (b) Psychometric curve with fitted function for absolute threshold experiment of pit spacing. (c) Experimental setup for perceiving different texture patterns. (d) Confusion matrix of experimental results for six basic texture patterns. (e) Accuracy of texture discrimination and average time of each participant for six basic texture patterns. (f) Confusion matrix of experimental results for four basic texture patterns. (g) Accuracy of texture discrimination and average time of each participant for four complex texture patterns.

absolute threshold of the pit spacing is 1.784 mm. Compared with the absolute threshold, the resolution of our tactile device is 1.5 mm, which means that our tactile device can render fine textures.

B. Texture patterns discrimination

To validate the performance of the MRS-Tex and explore its possible applications, we conducted two user studies in which two groups of participants were asked to respectively distinguish six basic texture patterns and four complex texture patterns (schematic diagram in Fig. 9, the actual undeformed/deformed photos in Fig. S5 and S6). As shown in Fig. 8(c), a participant was seated in front of a table and slid index finger of the right hand back and forth on the surface of MRS-Tex, just like perceiving the texture of objects in daily life. An NdFeB magnet with a surface flux density of 300 mT was used to generate an applied magnetic field. Under this magnetic field, the magnetic units sunk downward and formed pits on the surface of MRS-Tex.

Before the experiments, all the participants were interviewed. None of them reported any history of neurological illness or physical injury that might have affected their hand function. All participants signed a written consent to participate in the study, and the experiments were performed in consistent with the human participant testing regulations of the authors' institution.

For each participant, after five minutes of training, he/she perceived the randomly presented textures (six basic texture patterns or four complex texture patterns), and each texture was

TABLE I
COMPARISON BETWEEN OUR DEVICE AND OTHER TACTILE DEVICES IN TERMS OF FIVE MAIN FEATURES.

Tactile Device	Actuation Type	Spatial Resolution (mm)	Soft / Rigid (Actuator)	Stretchability	Vertical Displacement (mm)
[32]	DEA	4-6	Soft	Low	0.16
[18]	Pneumatic	23	Rigid	No	20
[19]	Pneumatic + SMP	4	Soft	No	0.50
[20]	Artificial muscle	8	Soft	High	0.45
[33]	Voice coil + magnet	2.50	Rigid	No	0.60
[34]	DFT	2.50	Soft	No	1.45
[17]	DEA	4	Rigid	No	0.35
Our	Soft actuator + coil	1.50	Soft	High	0.21

randomly presented 10 trials. By sliding the finger on the MRS-Tex surface, the participant identified the rendered texture and verbally reported which texture he/she perceived. Note that the participants were allowed to touch the presented textures as many times as they wanted. Throughout the experiment, the participants were blindfolded to prevent the interference from the visual texture cues.

In the first study, 12 right-handed participants (7 males and 5 females, aged from 22 to 35, with a mean age of 28.6) participated in the discrimination experiment of six basic texture patterns. A confusion matrix is used to report the experimental results (Fig. 8(d)), the values of units along the diagonal line are significantly greater than that of other units, and the sparse and dense stripes along the same orientation are relatively difficult to be distinguished. Furthermore, we calculated the accuracy of texture discrimination and the average time spent by each participant. As shown in Fig. 8(e), the accuracy of texture discrimination for each participant is higher than 85%, and the average time of each participant is less than 22 s (the minimum average time is 5.6 s).

For the second study, 12 right-handed participants (aged between 24 and 36, with an average age of 28.8) took part in the experiment. Similar to the experiment results of the six basic textures, the values along the diagonal line are significantly greater than the other values (Fig. 8(f)). As shown in Fig. 8(g), the discrimination accuracy of each participant is lower than 93%, and the average discrimination accuracy of 12 participants is 82.1%, which is not as high as the discrimination accuracy (92.5%) for six basic texture patterns. In addition, the average time (16.53 s) taken to discriminate these complex texture patterns was longer than that (12.26 s) taken to discriminate six basic texture patterns.

V. DISCUSSION

As shown in Fig. 5(c), the pit depth is 0.21 mm under the applied magnetic field of 300 mT. In addition, we found that when a magnetic unit is close to other magnetic units, under the same applied magnetic field, these clustered magnetic units will produce a larger downward movement distance compared with an isolated magnetic unit. We call this phenomenon the aggregation effect. To better understand this phenomenon, we measured the depth of pits generated in the sparse vertical stripes. The measurement results show that when the applied magnetic field is 300 mT, the average depth of pits can reach up to 0.47 mm (Fig. S7), which is far larger than the absolute threshold of the pit with a diameter of 1 mm. Therefore, the surface textures rendered by clustered magnetic units can be more easily perceived by users. In future work, we will further explore the aggregation effect so that the MRS-Tex can render richer surface textures.

The experiment results indicate that complex texture discrimination is more difficult than basic texture

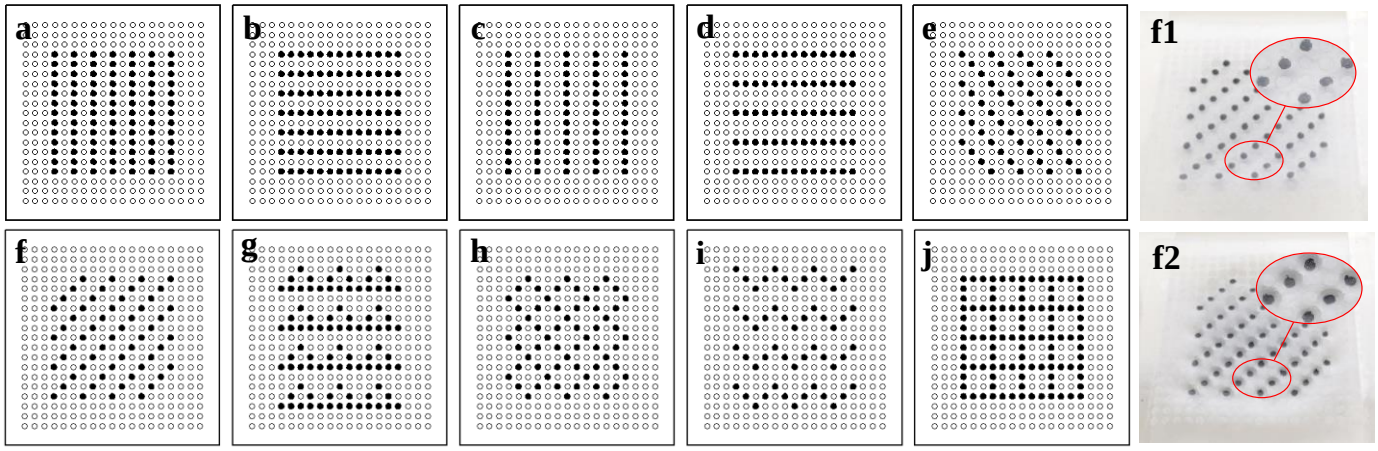

Fig. 9. Ten texture patterns for texture identification, including four six basic textures (a) dense vertical stripes (DVS), (b) dense horizontal stripes (DHS), (c) sparse vertical stripes (SVS), (d) sparse horizontal stripes (SHS), (e) left diagonal stripes (LDS) and (f) right diagonal stripes (RDS), and four complex textures (g) triangular stripes (TS), (h) diamond stripes (DS), (i) wave stripes (WS), (j) square stripes (SS). Taking RDS as an example, the actual undeformed/deformed photos of RDS are respectively shown in (f1) and (f2), and the actual undeformed/deformed photos of the remaining textures are shown in Fig. S5 and S6.

discrimination, and the latter has higher discrimination accuracy and less discrimination time. Nevertheless, even in the complex texture discrimination, the average discrimination accuracy of 12 participants is greater than 82% and the average time of 12 participants is less than 17 s, demonstrating that the textures formed by the MRS-Tex can be correctly distinguished in a short time. Moreover, from the user study, we found that the results of texture discrimination are related to the users' tactile perception ability. For example, in the first study, the accuracy of texture discrimination for the 12th participant is 100% and her average time is only 6.64 s (Fig. 9(e)). After the experiment, we learned that she is very sensitive to the materials such as clothes and sheets in daily life.

Compared with some typical tactile devices, the MRS-Tex has the features of millimeter-level spatial resolution (1.5 mm), flexibility, stretchability, and untethered actuation (Table I). Therefore, in addition to the 10 texture patterns depicted in Fig. 9, MRS-Tex also has the potential to form complex texture patterns, such as braille, numbers, letters, emotion state (Fig. S8), fabric textures, and embroidery texture. This will make MRS-Tex very useful to applications such as braille display, product design, emotional communication and virtual shopping. For example, our device can be used as a tool for evaluating the haptic sensation in the concept design phase of products such as the interior leather selection in automobile design. Our tactile device has the potential to assist the designer to evaluate whether the texture patterns have a desirable sensation. Furthermore, thanks to the excellent characterization (i.e., flexibility, stretchability, untethered actuation and miniaturization), MRS-Tex has the potential to be combined with other tactile modes such as softness and shape display to provide users with a rich multi-modal tactile experience.

VI. Conclusions and Future Work

In this paper, we proposed a novel tactile device, MRS-Tex, which can display textures on a soft thin film using a MRSA array and a soft membrane bracket. When a magnetic field is applied, the MRSA array generates pits on the thin film surface. Thanks to the proposed sunken solution and flexible magnetic actuators, the device can render textures in a spatial resolution of up to 1.5 mm with a sufficient holding force. The experimental validation shows that the MRS-Tex allows users to accurately distinguish between texture patterns when the MRSA array generates perceivable depth of pits.

To further explore the potential applications of MRS-Tex, we will prepare more complex textures on the device (such as brick texture and polygon texture) and evaluate the user experience. In addition, the aggregation effect mentioned in Section V will be further investigated so that the spatial resolution can be further improved, making it possible to display fine textures, such as that of cotton and silk.

References

[1] S. Yun, S. Park, B. Park, S. Ryu, S. M. Jeong, and K. Kyung, "A Soft and Transparent Visuo-Haptic Interface Pursuing Wearable Devices," IEEE T. Ind. Electron., vol. 67, DOI 10.1109/TIE.2019.2898620, no. 1, pp. 717-724, Jan. 2020.

[2] W. Park, E. Shin, Y. Yoo, S. Choi, and S. Kim, "Soft Haptic Actuator Based on Knitted PVC Gel Fabric," IEEE T. Ind. Electron., vol. 67, DOI 10.1109/TIE.2019.2918470, no. 1, pp. 677-685, Jan. 2020.

[3] Ó. Oballe-Peinado, J. A. Hidalgo-López, J. Castellanos-Ramos, J. A. Sánchez-Durán, R. Navas-González, J. Herrán, and F. Vidal-Verdú, "FPGA-Based Tactile Sensor Suite Electronics for Real-Time Embedded Processing," IEEE T. Ind. Electron., vol. 64, DOI 10.1109/TIE.2017.2714137, no. 12, pp. 9657-9665, Dec. 2017.

[4] G. Petit, A. Dufresne, V. Lévesque, V. Hayward, and N. Trudeau, "Refreshable Tactile Graphics Applied to Schoolbook Illustrations for Students with Visual Impairment," in 10th international ACM SIGACCESS conference on Computers and accessibility, DOI 10.1145/1414471.1414489, pp. 89-96, Oct. 2008.

[5] B. Duvernoy, I. Farkhatdinov, S. Topp, and V. Hayward, "Electromagnetic Actuator for Tactile Communication," in 2018 Eurohaptics Conference, DOI 10.1007/978-3-319-93399-3_2, pp. 14-24, Jun. 2018.

[6] H. Zhao, A. M. Hussain, A. Israr, D. M. Vogt, M. Duduta, D. R. Clarke, and R. J. Wood, "A Wearable Soft Haptic Communicator Based on Dielectric Elastomer Actuators," Soft Robot., DOI 10.1089/soro.2019.0113, Jan. 2020.

[7] X. Yu, Z. Xie, Y. Yu, J. Lee, A. Vazquezguardado, H. Luan, J. Ruban, X. Ning, A. Akhtar, and D. Li, "Skin-integrated wireless haptic interfaces for virtual and augmented reality," Nature, vol. 575, DOI 10.1038/s41586-019-1687-0, no. 7783, pp. 473-479, Nov. 2019.

[8] D. Wang, K. Ohnishi and W. Xu, "Multimodal Haptic Display for Virtual Reality: A Survey," IEEE T. Ind. Electron., vol. 67, DOI 10.1109/TIE.2019.2920602, no. 1, pp. 610-623, Jan. 2020.

[9] A. Withana, D. Groeger and J. Steimle, "Tacttoo: A Thin and Feel-Through Tattoo for On-Skin Tactile Output," in user interface software and technology, DOI 10.1145/3242587.3242645, pp. 365-378, Oct. 2018.

[10] T. Hui and J. B. D., "A microfabricated electrostatic haptic display for persons with visual impairments," IEEE T Rehabil Eng., vol. 6, DOI 10.1109/86.712216, no. 3, pp. 241-248, Sep. 1998.

[11] X. Guo, Y. Zhang, D. Wang, and J. Jiao, "Absolute and discrimination thresholds of a flexible texture display," in 2017 IEEE World Haptics Conference, DOI 10.1109/WHC.2017.7989913, pp. 269-274, Jun. 2017.

[12] R. L. Klatzky, S. Adkins, P. Bodas, R. H. Osgouei, S. Choi and H. Z. Tan, "Perceiving texture gradients on an electrostatic friction display," in 2017 IEEE World Haptics Conference, DOI 10.1109/WHC.2017.7989893, pp. 154-158, Jun. 2017.

[13] C. L. Van Doren, D. G. Pelli and R. T. Verrillo, "A device for measuring tactile spatiotemporal sensitivity," J. Acoust. Soc. Am., vol. 81, DOI 10.1121/1.394755, no. 6, pp. 1906-1916, Mar. 1987.

[14] X. Dai, J. E. Colgate and M. A. Peshkin, "LateralPaD: A surface-haptic device that produces lateral forces on a bare finger," in IEEE Haptics Symposium, DOI 10.1109/HAPTIC.2012.6183753, pp. 7-14, Mar. 2012.

[15] T. Nara, M. Takasaki, T. Maeda, T. Higuchi, S. Ando, and S. Tachi, "Surface acoustic wave tactile display," IEEE Comput. Graph, vol. 21, DOI 10.1109/38.963461, no. 6, pp. 56-63, Nov. 2001.

[16] A. Raza, W. Hassan, T. Ogay, I. Hwang, and S. Jeon, "Perceptually Correct Haptic Rendering in Mid-Air Using Ultrasound Phased Array," IEEE T. Ind. Electron., vol. 67, DOI 10.1109/TIE.2019.2910036, no. 1, pp. 736-745, Jan. 2020.

[17] H. Phung, C. T. Nguyen, T. D. Nguyen, C. Lee, U. Kim, D. Lee, J. Nam, H. Moon, J. C. Koo, and H. R. Choi, "Tactile display with rigid coupling based on soft actuator," Meccanica, vol. 50, DOI 10.1007/s11012-015-0270-5, pp. 2825-2837, Nov. 2015.

[18] M. A. Robertson, M. Murakami, W. Felt, and J. Paik, "A Compact Modular Soft Surface With Reconfigurable Shape and Stiffness," IEEE-ASME T. Mech., vol. 24, DOI 10.1109/TMECH.2018.2878621, no. 1, pp. 16-24, Feb. 2019.

[19] N. Besse, S. Rosset, J. J. Zarate, and H. Shea, "Flexible Active Skin: Large Reconfigurable Arrays of Individually Addressed Shape Memory Polymer Actuators," Adv Mater Technol-Us., vol. 2, DOI 10.1002/admt.201700102, no. 10, pp. 1700102, Aug. 2017.

[20] C. Lamuta, H. He, K. Zhang, M. Rogalski, N. R. Sottos, and S. H. Tawfick, "Digital Texture Voxels for Stretchable Morphing Skin Applications," Adv Mater Technol-Us., vol. 4, DOI 10.1002/admt.201900260, no. 8, pp. 1900260, May. 2019.

[21] F. Vidal-Verdu and M. Hafez, "Graphical Tactile Displays for Visually-Impaired People," IEEE T. Neur. Sys. Reh., vol. 15, DOI 10.1109/TNSRE.2007.891375, no. 1, pp. 119-130, Mar. 2007.

[22] C. J. Camargo, H. Campanella, J. E. Marshall, N. Torras, K. Zinoviev, E. M. Terentjev, and J. Esteve, "Batch fabrication of optical actuators using nanotube–elastomer composites towards refreshable Braille displays," J. Micromech. Microeng., vol. 22, DOI 10.1088/0960-1317/22/7/075009, no. 7, pp. 075009, Jun. 2012.
[23] N. Torras, K. Zinoviev, C. J. Camargo, E. M. Campo, H. Campanella, J. Esteve, J. E. Marshall, E. M. Terentjev, M. Omastova, and I. Krupa, "Tactile device based on opto-mechanical actuation of liquid crystal elastomers," Sensor. Actuat. A-Phys., vol. 208, DOI 10.1016/j.sna.2014.01.012, pp. 104-112, Jan. 2014.
[24] A. Richter and G. Paschew, "Optoelectrothermic Control of Highly Integrated Polymer - Based MEMS Applied in an Artificial Skin," Adv. Mater., vol. 21, DOI 10.1002/adma.200802737, no. 9,pp. 979-983, Mar. 2009.
[25] W. Lee, J. Nam, B. Jang, and G. Jang, "Selective Motion Control of a Crawling Magnetic Robot System for Wireless Self-Expandable Stent Delivery in Narrowed Tubular Environments," IEEE T. Ind. Electron., vol. 64, DOI 10.1109/TIE.2016.2580126, no. 2, pp. 1636-1644, Feb. 2017.
[26] W. Lee, J. Nam, J. Kim, E. Jung, and G. Jang, "Effective Locomotion and Precise Unclogging Motion of an Untethered Flexible-Legged Magnetic Robot for Vascular Diseases," IEEE T. Ind. Electron., vol. 65, DOI 10.1109/TIE.2017.2726973, no. 2, pp. 1388-1397, Feb. 2018.
[27] H. Lu, M. Zhang, Y. Yang, Q. Huang, T. Fukuda, Z. Wang, and Y. Shen, "A bioinspired multilegged soft millirobot that functions in both dry and wet conditions," Nat. Commun., vol. 9, DOI 10.1038/s41467-018-06491-9, no. 1, pp. 3944, Sep. 2018.
[28] Y. Kim, G. A. Parada, S. Liu, and X. Zhao, "Ferromagnetic soft continuum robots," Sci Robot., vol. 4, DOI 10.1126/scirobotics.aax7329, no. 33, pp. eaax7329, Aug. 2019.
[29] W. Hu, G. Z. Lum, M. Mastrangeli, and M. Sitti, "Small-scale soft-bodied robot with multimodal locomotion," Nature, vol. 554, DOI 10.1038/nature25443, no. 7690, pp. 81-85, Jan. 2018.
[30] J. M. Loomis, "On the tangibility of letters and braille," Percept Psychophys., vol. 29, DOI 10.3758/BF03198838, pp. 37-46, Jan. 1981.
[31] L. A. Jones and H. Z. Tan, "Application of Psychophysical Techniques to Haptic Research," IEEE T. Haptics., vol. 6, DOI 10.1109/TOH.2012.74, no. 3, pp. 268-284, Dec. 2012.
[32] Ankit, N. Tiwari, M. Rajput, N. A. Chien, N. Mathews, "Highly Transparent and Integrable Surface Texture Change Device for Localized Tactile Feedback," Small, vol. 14, DOI 10.1002/smll.201702312, no. 1, pp. 1702312, Nov. 2017.
[33] J. Kim, B. K. Han, D. Pyo, S. Ryu, H. Kim and D. S. Kwon, "Braille Display for Portable Device Using Flip-Latch Structured Electromagnetic Actuator," IEEE T. Haptics., vol. 13, DOI 10.1109/TOH.2019.2963858, no. 1, pp. 59-65, Jan. 2020.
[34] A. K. Han, S. Ji, D. Wang and M. R. Cutkosky, "Haptic Surface Display based on Miniature Dielectric Fluid Transducers," IEEE Robot. Autom. Let., vol. 5, DOI 10.1109/LRA.2020.2985624, no. 3, pp. 4021-4027, Jul. 2020.

Yuan GUO received a M.E. degree in mechanical engineering in 2015, from Chongqing Jiaotong University, Chongqing, China. Currently he is working towards a Ph.D. degree in School of Mechanical Engineering and Automation at Beihang University, Beijing, China. His research interests include haptics, human-machine interaction, force feedback glove, VR, and robotics.

Qianqian TONG received her Ph.D. degree in School of Computer Science from Wuhan University, Wuhan, China in 2019. Currently she is a Postdoctoral Fellow at Peng Cheng Laboratory, Shenzhen, China. Her research interests include haptic rendering, haptic human-machine interface, and medical imaging analysis. She is an IEEE Member.

Xianzhong LIU was born in Beijing, China. Majoring in mechanical engineering, he is currently a senior student at the School of General Engineering, Beihang University, China. His research interests include haptic device and robot mechanism.

Xuesong BIAN was born in Dezhou, China. He received his B.S degree in School of Mechanical Engineering and Automation from Beihang University, Beijing, China in 2019. Currently he is pursuing his Master degree in School of Mechanical Engineering and Automation at Beihang University. His research interests include human machine interaction and haptic device.

Zhihao ZHANG was born in Yichun, Jiangxi Province, China in 1997. He received his bachelor's degree at the School of Mechanical Engineering and Automation, Beihang University, China. Currently he is working toward the M. degree of mechanical engineering in Beihang University, China. His interests include robot engineering and haptic device.

Yuru ZHANG (M'95-SM'08) received her Ph.D. degree in mechanical engineering from Beihang University, Beijing, China in 1987. Currently she is a professor at the State Key Laboratory of Virtual Reality Technology and Systems, Beihang University. Her technical interests include haptic human-machine interface, medical robotic systems, robotic dexterous manipulation, and virtual prototyping. She is a senior member of IEEE, and a member of ASME.

Weiliang XU (SM'99) received the B.E. degree in manufacturing engineering and the M.E. degree in mechanical engineering from Southeast University, Nanjing, China, in 1982 and 1985, respectively, and the Ph.D. degree in mechatronics and robotics from the Beijing University of Aeronautics and Astronautics, Beijing, China, in 1988. He joined The University of Auckland, Auckland, New Zealand, on February 1, 2011, as Chair in Mechatronics Engineering.

Dangxiao WANG (M'05-SM'13) received his Ph.D. degree in mechanical engineering from Beihang University, Beijing, China in 2004. Currently he is a professor at the State Key Laboratory of Virtual Reality Technology and Systems in Beihang University. From 2006 to 2016, he was an Assistant and Associate Professor in the School of Mechanical Engineering and Automation, Beihang University. His research interests include haptic rendering, NeuroHaptics and medical robotic systems. He is a senior member of IEEE. He had been an Associate Editor of IEEE Transactions on Haptics from 2015 to 2018. He had been the chair of Executive Committee of the IEEE Technical Committee on Haptics (IEEE TCH) from 2014 to 2017.